ELSEVIER

Brine entrainment in multistage flash desalination

Hisham Ettouney

Department of Chemical Engineering, Kuwait University, P.O. Box 5969, Safat 13060, Kuwait
email: hisham@kuc01.kuniv.edu

Abstract

Brine entrainment in the multistage flash desalination depends on the stage temperature. In the once through and the brine circulation systems, brine entrainment is high in the low temperature stages. In the brine circulation system and during winter operation, decrease in the feed seawater temperature requires operation of the cooling seawater recycle pump. This is to control the intake seawater temperature. Adoption of this technique might not be the optimum choice. This is because of the short duration of the winter period. Also, preparation and maintenance of this large size pump might not be technically feasible and would come at very high cost. Failure to operate the cooling seawater pump results in large increase in the product salinity. Therefore, it is necessary to extract product water from the first stages to supply the makeup boiler water. In the once through system, there is no control on the feed seawater temperature. Therefore, the product salinity increases during winter operation. This would also call for product extraction from the high temperature stages. makeup water. Parametric analysis is presented for variations in the product salinity as a function of the feed seawater temperature.

Keywords: Demister; Multistage flash desalination; Once through; Brine circulation; Vapor entrainment

1. Introduction

Demisting of vapor or gas streams is a very important industrial process. Carry over liquid droplets or mist is not desirable since it would affect the product purity. In distillation columns, the enriched vapor stream rising in the column might carry over liquid droplets, which are not of the same composition as the vapor stream. As a result, the condensate product might not be of the desired composition or quality. In thermal desalination processes, the flashed or boiled vapor may entrain brine droplets, which would result in higher salt concentration in the product stream.

Several configurations can be used for mist or droplet removal; these include settling tanks, filters, electrostatic precipitators, cyclones, baffles/vanes, and wire mesh demisters. Selection among these devices depends

on the composition of the mist/droplets, size, flow rate, and temperature. Originally, the thermal desalination processes did not utilize any form of mist or droplet removal [1]. As result, the product salinity was found to fluctuate over a wide range. In some instances, such large variations were not a problem as long as the water use was limited to households, agriculture, or industrial processes. However, water use as a makeup feed for boilers requires stricter limits. This is to prevent rapid consumption of the water polishing chemicals or exhaustion of the ion-exchange and demineralization resins. In the late 1950s baffles were introduced in the last flashing stage of the MSF [1]. This has lead to some improvement of the product quality. However, the product quality was not tightly controlled. In addition, the baffles/vanes caused large pressure drop in the vapor stream, which resulted in decrease of the vapor temperature. These drawbacks are eliminated through the use of wire mesh demisters, which was installed in all stages. Proper design of the wire mesh demisters is found to provide close to 100% mist elimination. In addition, pressure drop across the demisters is almost negligible, as long as the demister is kept in clean conditions.

Rognoni et al. [2] presented an innovative system for spray enhanced demisting, which reduces the product salinity to values below 0.1 ppm. The proposed system includes two demister pads in addition to the distillate spray system. The proposed system is thought to maintain high quality distillate and to eliminate the down stream polishing units, i.e., ion exchange resins.

A limited number of literature studies is found on demister performance evaluation or modeling. The common design procedure for vapor release velocity and the vapor velocity within the demister is given by

$$v_{\mathrm{v}} = k \left(\frac{\rho_l - \rho_{\mathrm{v}}}{\rho_{\mathrm{v}}} \right)^{0.5} \tag{1}$$

Values for the k constant are reported equal to 0.058 and 0.078, for the vapor release velocity and the vapor velocity within the demister, respectively [3]. Use of Eq. (1) is not practical, since, it would require prior knowledge of the k value. Careful evaluation of the k value might require careful experimentation and measurements over a range of temperature and vapor velocities. An empirical correlation is developed by El-Dessouky et al. [4] for removal efficiency of large mist droplets. This correlation has monotonic dependence on the vapor velocity, which limits its use to the droplet capture.

A better approach for demister design is found in the study by Brunazzi and Pagliani [5]. They have presented a semi-empirical model for the demister design. The model builds on previous analysis presented by Langmuir and Blodgett [6], Pich [7], who evaluated the inertial capture efficiency for a single wire, expressed in terms of a dimensionless stokes number. The analysis for industrial wire mesh packing is presented by Carpenter and Othmer [8] as a function of the demister pad thickness, the demister specific area, the stocks efficiency, and the number of mesh layers. The semi-empirical approach is further revised by Brunazzi and Paglianti [5]. They performed experimental and mathematical analysis for the removal of fine mist particles. The analysis is presented as a function of various design and operating parameters. The equation presented by Brunazzi and Paglianti [5] fits well the experimental data; however, it is limited to the range of droplet capture. The correlation does not take into account effects of very large vapor velocity, were droplet detachment and re-entrainment into the vapor stream takes place.

This study focuses on droplet and mist re-entrainment from the demister, which occurs for large vapor velocities. This condition may arise due to reduction in the intake seawater temperature and subsequent reduction in the brine temperature in the last flashing stages. The analysis is presented as a function of the stage temperature and other demister properties.

2. MSF flashing stage

This section includes brief description of the MSF flashing stage; more detailed discussion, modeling, and analysis can be found in the textbook by El-Dessouky and Ettouney on desalination processes [9]. A schematic for the MSF flashing stage is shown in Fig. 1. Critical design elements of the flashing stage includes the stage dimensions, the demister, the brine orifice, venting lines, and the condenser tube bundle. The width of the flashing stage is set by the brine load or the flow rate of brine per one meter. Low loads would affect brine mixing, which may reduce the bubble formation and release rates. Higher loads are not either desirable; this condition might cause vibrations

within the flashing stage increase the erosion rates of the brine gate and splash plate.

The length of the flashing stage together with its width sets the stage cross section area. This design parameter together with the flashing rate within the stage sets vapor velocity, which in turn affects the ratio of entrained/settled brine droplets. The demister design depends on two important factors that affect the demister efficiency; the first is the distance between the demister and the top of the brine pool. Small distances would imply reduction of the settling length of the brine droplets. A large distance is not also desirable, because of the increase of energy losses as well as the cost of stage and the system foundations. A distance of 2 m between the lower face of the demister and top of the brine is found to provide sufficient length for settling of brine droplets. The second factor is the demister area; which is set to limit the vapor velocity between 4 and 5 m/s, especially at low temperature stages. Smaller areas would result in large vapor velocity within the demister. This would result in the increase of the re-entrainment rate of the brine droplets and subsequent increase of the product salinity.
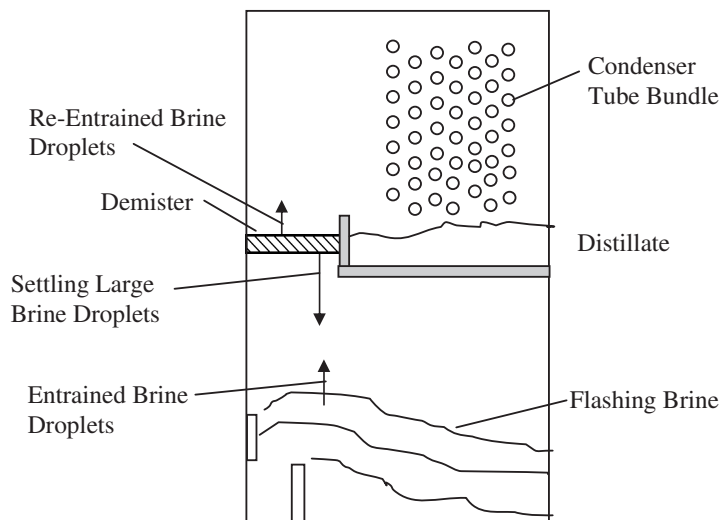

Fig. 1. Schematic of the MSF flashing stage.

Buoyancy, m g ρ_v

Drag, $\pi R^2 v^2/2$

Gravity, m g ρ_l

Buoyancy, m g ρ_v
Buoyancy, m g ρ_v

Drag, $\pi R^2 v^2/2$

Demister wires

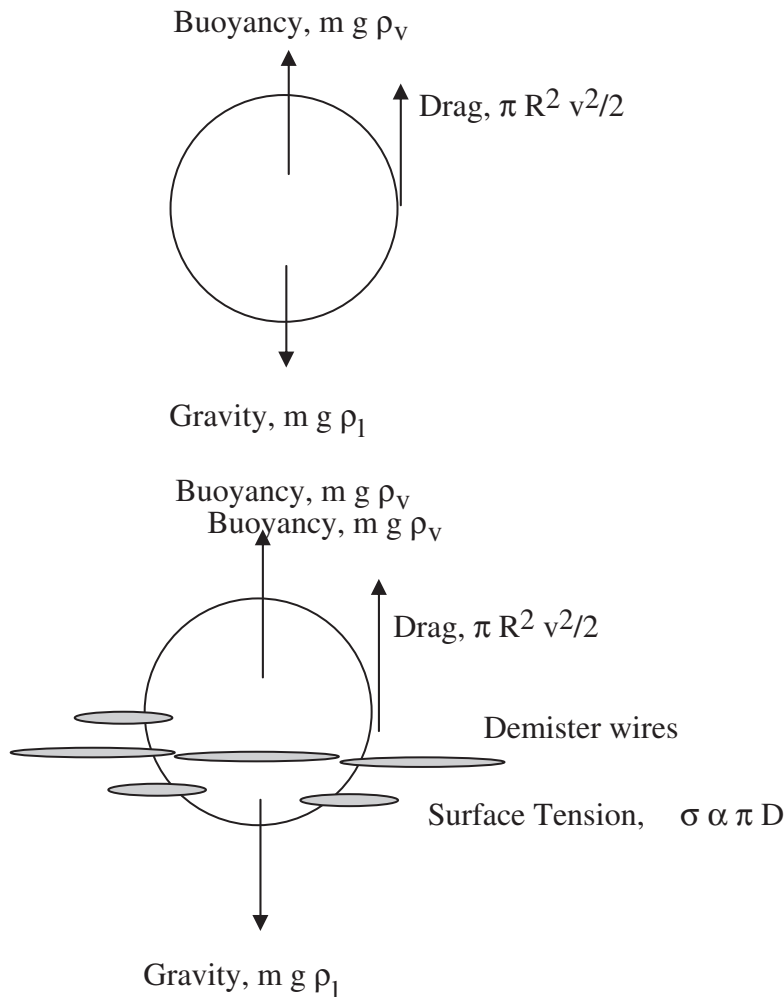Surface Tension, $\sigma \alpha \pi D$

Gravity, m g ρ_l

Fig. 2. (a) Balance of forces for a settling liquid droplets. (b) Balance of forces for a droplet attached to a demister wire.

The remaining system dimensions to be set include the thickness of demister pad and the height of the flashing stage. The thickness of the demister pad is usually set at 0.15–0.2 m. The thickness of the demister pad together with the wire diameter and the number of wire layers have a strong effect on the demister removal efficiency. The stage height should accommodate the required height for the flashing brine pool, which is about 0.4 m. That height includes 0.2 m for the height of the brine gate and 0.2 m for the brine height above the gate. Also, the stage height includes 2 m for the distance between the top of the brine pool and the demister. The remaining length of the stage height should accommodate the condenser tube bundle.

3. Settling velocity and critical droplet diameter

Droplet settling velocity and the critical droplet diameter, which is defined as the smallest

droplet diameter that would settle by gravity within the flashing stage. Both parameters are obtained through balance of forces on brine droplets traveling between the brine surface and the lower face of the demister. This requires droplets forces balance, which includes, drag, buoyancy, and gravity, which is shown in Fig. 2(a). This balance is given by

$$\frac{\pi d_d^2}{4} C_d \rho_v v_v^2 = \frac{1}{6} \pi d_d^3 (\rho_l - \rho_v) g \tag{2}$$

The general form of the drag coefficient used in Eq. (2) is given by

$$C_d = \frac{24}{Re} + \frac{3}{Re^{0.5}} + 0.34 \tag{3}$$

The critical droplet diameter is obtained from Eq. (2) for an MSF system operating at the conditions given in Table 1. Figure 3 shows variations in the critical droplet diameter as a function of the stage number. The figure also shows variations in the vapor velocity as a function of the stage number. In addition, the droplet settling velocity is obtained as a function of the stage number and the droplet diameter.

The results shown in Fig. 3 shows that the critical droplet diameter varies over a range of 10–80 mm. This is associated with a velocity range of 1–5 m/s. It should be noted that these calculations are obtained for an intake seawater temperature of 34°C and brine reject temperature of 40°C.

4. Semi-empirical models

Semi-empirical models are found in the works by Carpenter and Othmer [7] and Brunazzi and Paglinati [3]. Both models are based on the Stokes number, which is given by

$$St = \frac{\rho_l v d_d^2}{18 \mu_v d_w} \tag{4}$$

Common assumptions for the two models include no re-entrainment from the demister into the vapor stream and no-build up of liquid within the demister. The first assumption is the main shortcoming in all of these since it overlooks an important physical aspect of demister design and operation. The second assumption implies steady state operation, which is the case for normal operation; this is other than startup, shutdown, or during change of operating conditions. Brunazzi and Paglinati [5] assumed also assumed no mixing after vapor passage through each layer of the demister.

The Carpenter and Othmer [8] suggested the following semi-empirical equation

$$\eta_n = 1 - \left(1 - \frac{2}{3} A_p \eta_{ST} \frac{H_p}{\pi}\right)^n . \tag{5}$$

The stocks number efficiency (η_{ST}) is defined by the following relations

$$\eta_{ST} = St \text{ for } St \leq 1 \tag{6}$$

$$\eta_{ST} = 1 \text{ for } St \geq 1 \tag{7}$$

Equation (5) shows increase in the droplet removal efficiency upon increase in the vapor velocity, the droplet diameter, the demister pad thickness, and the demister specific area, and the number of layer in the demister. On the other hand, the removal efficiency decreases with the increase in the demister wire diameter and temperature.

The following equations is proposed by Brunazzi and Paglianti [5]

Table 1
Variation in the removal efficiency as a function of various operating and design parameters

T_v °C	d_d m	ϵ	d_w mm	v_v m/s	H_p mm	n_p	A_p mm²/mm³	St	η_{St}	η_n [6]	η_n [3]
40	5×10^{-6}	0.98	0.27	1	150	28	0.267	0.530	0.530	0.992	0.910
50	5×10^{-6}	0.98	0.27	1	150	28	0.267	0.506	0.506	0.990	0.895
60	5×10^{-6}	0.98	0.27	1	150	28	0.267	0.485	0.485	0.988	0.880
50	5×10^{-6}	0.98	0.27	1	150	28	0.267	0.506	0.506	0.990	0.895
50	7×10^{-6}	0.98	0.27	1	150	28	0.267	0.993	0.993	0.999	1
50	9×10^{-6}	0.98	0.27	1	150	28	0.267	1.642	1	0.999	1
50	5×10^{-6}	0.98	0.27	1	150	28	0.267	0.506	0.506	0.990	0.895
50	5×10^{-6}	0.95	0.27	1	150	28	0.267	0.506	0.506	0.990	0.901
50	5×10^{-6}	0.92	0.27	1	150	28	0.267	0.506	0.506	0.990	0.908
50	5×10^{-6}	0.98	0.23	1	150	28	0.267	0.595	0.595	0.996	0.943
50	5×10^{-6}	0.98	0.25	1	150	28	0.267	0.547	0.547	0.993	0.920
50	5×10^{-6}	0.98	0.27	1	150	28	0.267	0.506	0.506	0.990	0.895
50	5×10^{-6}	0.98	0.27	2	150	28	0.267	1.013	1	0.999	1
50	5×10^{-6}	0.98	0.27	3	150	28	0.267	1.520	1	0.999	1
50	5×10^{-6}	0.98	0.27	4	150	28	0.267	2.027	1	0.999	1
50	5×10^{-6}	0.98	0.27	1	100	28	0.267	0.506	0.506	0.951	0.777
50	5×10^{-6}	0.98	0.27	1	150	28	0.267	0.506	0.506	0.990	0.895
50	5×10^{-6}	0.98	0.27	1	200	28	0.267	0.506	0.506	0.998	0.950
50	5×10^{-6}	0.98	0.27	1	150	20	0.267	0.506	0.506	0.992186	0.895435
50	5×10^{-6}	0.98	0.27	1	150	24	0.267	0.506	0.506	0.991335	0.895435
50	5×10^{-6}	0.98	0.27	1	150	28	0.267	0.506913	0.506	0.990703	0.895435
50	5×10^{-6}	0.98	0.27	1	150	28	0.267	0.506913	0.506	0.990703	0.895435
50	5×10^{-6}	0.98	0.27	1	150	28	0.217	0.506913	0.506	0.976258	0.836127
50	5×10^{-6}	0.98	0.27	1	150	28	0.367	0.506913	0.506	0.99871	0.954974

$$\eta_n = 1 - (1 - \eta_{ST})^M \left[\frac{\bar{n} - n'}{\bar{n}} + \frac{n'}{\bar{n}}(1 - \eta_{ST}) \right] \quad (8)$$

The parameters $\bar{n}$ depends on the demister wire diameter, the demister porosity, the number of demister layers, the demister length, and specific demister area. Expressions for $\bar{n}$ and n' can be found in ref [5].

Variations in the removal efficiency are shown in Table 2 as a function of the vapor temperature, droplet diameter, demister porosity, wire diameter, demister pad thickness, number of demister layers, demister specific area, and vapor velocity. As is shown, there is large discrepancies between the three models especially at low velocities and small droplet diameter. The removal efficiency for the two models becomes similar upon the increase in

the vapor velocity, droplet diameter, and the specific area.

5. Modeling of settling/re-entrained droplet

Flow of brine droplets in the distillate vapor is affected by several parameters, which includes the stage or vapor temperature, the range of droplets diameter, and the salinity of the droplets. Several mechanisms affect the motion of the brine droplets upon their release from the surface of the flashing brine and until reaching the lower surface of the demister. Fine and small droplets may coalesce to form larger size droplets. Once the particle size exceeds a certain limit it will start to settle back to the brine pool. This is because its settling velocity would become larger than the vapor velocity, once its size exceeds a certain limit. Also, droplets may
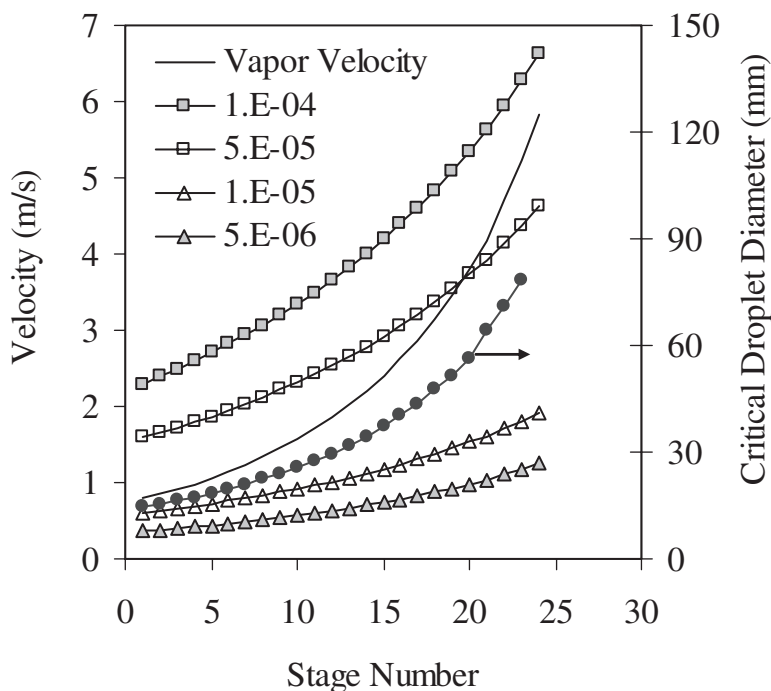

Fig. 3. Variation in the vapor and the droplet settling velocity as a function of the particle diameter and the stage number for the MSF process. ——, Vapor velocity; —□—, 1.E-04; —□—, 5.E-05; —△—, 1.E-05; —△—, 5.E-06.

Table 2
MSF and demister design parameters

Parameter	Value	Units
X_b	70000	ppm
X_f	36000	ppm
T_{cw}	15	°C
T_{b_n}	21	°C
ΔT_l	1.5	°C
C_p	4.2	kJ/kg K
U_h	2.48	kW/(m^2 K)
U_{c_r}	2.19	kW/(m^2 K)
U_{cj}	2.12	kW/(m^2 K)
H_p	2.12	kW/(m^2 K)
A_p	0.267	kW/(m^2 K)
ϵ_p	0.98	
n_s	24	
n_j	3	
T_{b_o}	90	°C
T_s	100	°C
v_v	4	m/s
w	180	kg/(m s)
M_d	378	kg/s
T_{f_1}	83.5	°C
d_w	mm	0.27
d_d	5×10^{-6}	m
n_p	28	

reduce their size as a result of water evaporation from their surface to the surrounding vapor.

As the vapor/droplets flow through the demister, the droplets are captured and accumulated on the surface of the demister wires. The brine droplets are captured on the wires because of their larger density. The vapor stream can bend around the demister wires, while, the brine droplets would continue to flow in a straight line. As a results, the droplets would hit the demister wires and loss their momentum. Droplet accumulation might result in increase of the droplet size or formation of a small thin film. As the size of the droplets captured by the demister wires increase it may starts to detach from the wire and drop back to the brine pool.

The vapor velocity is set by the stage dimensions and temperature. Since the stage dimensions are unaltered then the only thing that would change the vapor velocity is the brine temperature. This occurs during winter operation, where, the feed water temperature may drop to values below 20 °C. This would result in reduction in the stage pressure and large increase in the vapor specific volume and the vapor velocity. As a result, the critical size for the droplets to settle increases. Also, the drag effects of the vapor flowing in the demister would increase to the point that droplets would detach from the wire surface and entrains in the rapidly moving vapor stream.

Various forms can be assumes for the liquid shape covering the demister wires. For

example, a whole liquid drop can be assumed to be trapped within the demister wires. Also, a liquid film with a perfect or partial cylindrical shape can be assumed. The condition considered in the analysis is that for liquid droplet. Figure 2(b) shows a brine droplet entrained by the demister wires. The droplet experiences the balance of the following forces; surface tension, drag, gravity, and buoyancy. For a droplet to be re-entrained in the vapor stream the drag and buoyancy must be equal to or greater than the gravity and surface tension adhesion. The force balance on a stationary droplet at this critical condition is given by

$$\frac{\pi d_d^2}{4} C_d \rho_v v_v^2 = \pi d_d \alpha \sigma + \frac{1}{6} \pi d_d^3 (\rho_l - \rho_v) g \qquad (9)$$

In Eq. (9) the drag coefficient is given by Eq. (3). The parameter α appearing on the right hand side of Eq. (9) is used to define the fraction of the droplet perimeter which is attached to the demister wires. At the re-entrainment point the vapor velocity passing through the demister should be greater the vapor velocity obtained from Eq. (9). It should be noted that Eqs. (9) and (3) would give a specific critical velocity, which applies a specific droplet diameter. A Gaussian distribution for the droplet particle diameter can be used to obtain an average value for the critical velocity. The resulting ratio of the critical re-entrainment velocity together with the actual vapor velocity can be used to determine the fraction of re-entrained vapor.

At steady state conditions, the demister wire will be covered by a thin layer of liquid brine. The mass the liquid brine covering the demister wires can be obtained as a function of the demister specific area and by assume the fraction of the wires covered by the liquid brine and the thickness of the liquid film.

Therefore, the mass of the brine covering the demister wires is given by

$$m_b = \alpha_2 A_p V_p \delta_f \rho_b \qquad (10)$$

In Eq. (10), the parameter α_2 defines the fraction of the demister area covered by liquid brine. The demister volume (Vp) is obtained through definition of the demister length, height, and width.

The rate of brine re-entrainment is obtained by dividing the brine mass given by Eq. (10) by the vapor residence time within the demister, which is given by

$$\tau = \frac{\rho_b L_p W_p H_p}{D_i} \qquad (11)$$

Figure 4 shows the variation in the product salinity for an MSF system with 24 stages. The results are shown as a function of the intake seawater temperature. The calculations assumes that the entrainment results for an MSF system with 24 stages. The system is designed at the conditions shown in Table 1. As is shown in Fig. 4, the product salinity remains within limits at values below 25 ppm as long as the intake seawater temperature is above 30 °C. Rapid increase the product salinity occurs as the intake seawater temperature drops to values of 20 and 15 °C. Another feature of these results is that most of the salinity increase in the product water occurs in the low temperature stages; especially, in the heat rejection section and the last stages in the heat recovery section.

6. Conclusions

Design and analysis of various elements of the desalination processes is an essential part in process development. In this study focus is made on design and performance analysis of the wire mesh demister. The results presented
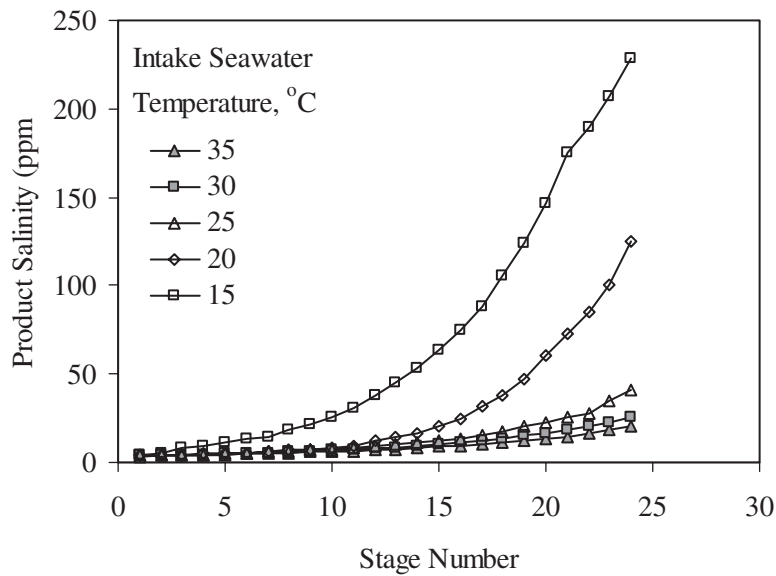
Fig. 4. Variation in the product salinity as a function of the intake seawater temperature and the stage number. Intake seawater temperature, °C:—▲—, 35;—▫—, 30;—▲—, 25;—◇—, 20;—▫—, 15.

in this study show the complexity of such system. A fully empirical or semi-empirical approach to address system design and performance evaluation is the only feasible mean for development of useful design equations. In either case, experimentation requires careful execution, detailed measurements for a number of parameters that include droplet radius, vapor velocity, temperature, and other characteristics of the demister pad (length, packing density, wire diameter, and specific area).

An important finding in this analysis is the possibility to operate the brine circulation MSF without the need the winter time temperature control loop. Although, would increase the final product salinity, which might not be suitable for use a boiler make up water. This problem can be either addressed by the use of an RO system to reduce the feed water salinity from high values of 200–400 to practical limits of less than 10 ppm. Another approach might be the use of product water generated in the first few stages, where the salinity remain less than 10 ppm.

Nomenclature

$A\text{p}$	—	Demister specific area, m^2/m^3.
C_d	—	Drag Coefficient, dimensionless.
d_d	—	Diameter of brine droplet, mm d_w Diameter of the wire, mm.
D_i	—	Mass flow rate of distillate product in stage i, kg/s g Gravitational acceleration, m/s^2.
$H\text{p}$	—	Thickness of demister pad, mm.
$L\text{p}$	—	Length of demister pad, mm.
M_d	—	Total mass flow rate of distillate product, kg/s.
n_s	—	Number of flashing stages.
n_j	—	Number of flashing stages in the heat rejection section.
n_p	—	Number wire mesh layers.
Re	—	Reynolds number of settling droplet, $Re = \frac{\rho_\text{v} v_\text{v} d_\text{d}}{\mu_\text{v}}$, dimensionless.

St — Stokes number, $St = \frac{\rho_l v d_d^2}{18 \mu_v d_w}$, dimensionless.

T_{cw} — Intake seawater temperature, °C.

T_{b_n} — Brine reject temperature, °C.

T_{f_1} — Brine temperature entering the brine heater, °C.

T_o — Top brine temperature, °C.

T_s — Heating steam temperature, °C.

ΔT_l — Average temperature losses per stage, °C

U_{cj} — Overall heat transfer coefficient in the condenser tubes in the heat rejection section, kW/m² K.

U_{c_r} — Overall heat transfer coefficient in the condenser tubes in the heat recovery section, kW/m² K

U_h — Overall heat transfer coefficient, kW/m² K.

V_p — Volume of demister pad, m³.

v_v — Vapor velocity, m/s.ll

w — Orifice loading, kg/(m s).

Wp — width of demister pad, mm.

X_b — Brine salinity, ppm.

X_f — Feed seawater salinity, ppm

Greek Symbols

η_{ST} — Demister separation efficiency defined by constraints of . (2).

η_n — Demister separation efficiency given by Eqs. (2) and (3).

σ — Surface tension, N/m.

ϵ_p — Demister porosity.

ρ_p — Demister packing density, kg/m³

ρ_l — Liquid density, kg/m³

ρ_v — Vapor density, kg/m³

μ_v — Dynamic viscosity of vapor, kg/(m s).

References

[1] Al-Zubaidi, Sea water desalination in Kuwait – a report on 33 years experience. Desalination, 63 (1987) 1–55.

[2] M. Rognoni, A. Trezzi and P. Lucchi, Spray enhanced demisting (SED). Desalination, 152 (2002) 185–190.

[3] K. Wangnick, How incorrectly determined physical and constructional properties in the seawater and brine regimes influence the design and size of an MSF desalination plant – stimulus for further thoughts. Proceedings of the IDA, World Congress on Desalination and Water Science, Abu Dhabi, 2, 1995, 201–218.

[4] H.T. El-Dessouky, I.M. Alatiqi, H.M. Ettouney and N.S. Al-Deffeeri, Performance of wire mesh mist eliminator. Chem. Eng. & Proc., 39 (2000) 129–139.

[5] E. Brunazzi and A. Paglianti, Design of wire mesh mist eliminators. AIChE J., 44 (1998) 505–512.

[6] I. Langmuir and K.B. Blodgett, U.S. Army Air Forces Technical Report, 5418 (1946).

[7] J. Pich, aerpsp Science, Chap. 9. C.N. Davies, ed., Academic Press, New York, 1966.

[8] C.L. Carpenter and D.F. Othmer, Entrainment removal by a wire-mesh separator. AIChE J., 1 (1955) 549.

[9] H. El-Dessouky and H.M. Ettouney, Fundamentals of Salt Water Desalination. Elsevier, ISBN: 0–444–50810–4, February 2002.